







Impact of physio-chemical spinning conditions on the mechanical properties of biomimetic spider silk fibers

Benjamin Schmuck ^{1,2}, Gabriele Greco ^{2,3}, Fredrik G. Bäcklund¹, Nicola M. Pugno ^{3,4}, Jan Johansson¹ & Anna Rising ^{1,2}

Artificial spider silk has emerged as a biobased fiber that could replace some petroleum-based materials that are on the market today. Recent progress made it possible to produce the recombinant spider silk protein NT2RepCT at levels that would make the commercialization of fibers spun from this protein economically feasible. However, for most applications, the mechanical properties of the artificial silk fibers need to be improved. This could potentially be achieved by redesigning the spidroin, and/or by changing spinning conditions. Here, we show that several spinning parameters have a significant impact on the fibers' mechanical properties by tensile testing more than 1000 fibers produced under 92 different conditions. The most important factors that contribute to increasing the tensile strength are fast reeling speeds and/or employing post-spin stretching. Stretching in combination with optimized spinning conditions results in fibers with a strength of >250 MPa, which is the highest reported value for fibers spun using natively folded recombinant spidroins that polymerize in response to shear forces and lowered pH.

¹Department of Biosciences and Nutrition, Karolinska Institutet, Neo, 141 83, Huddinge, Sweden. ²Department of Anatomy, Physiology and Biochemistry, Swedish University of Agricultural Sciences, Box 7011, 750 07 Uppsala, Sweden. ³Laboratory of Bio-Inspired, Bionic, Nano, Meta, Materials & Mechanics, Department of Civil, Environmental and Mechanical Engineering, University of Trento, Via Mesiano, 77, 38123 Trento, Italy. ⁴School of Engineering and Materials Science, Queen Mary University of London, Mile End Road, London E1 4NS, UK. ✉email: benjamin.schmuck@ki.se; anna.rising@ki.se

To master the art of spinning artificial spider silk has been a scientific challenge for more than 90 years^{1,2}. This long-term ambition to replicate one of nature's toughest materials³ indicates the difficulties associated with this task⁴. The main obstacles have been low yields from microorganism expression systems, difficulties to maintain the spidroins in a soluble state at high concentrations before spinning, and the inability to replicate the molecular processes that dictate spidroin assembly into a fiber^{2,5–11}. Still, the prospect of applying this lightweight but tough material in high-end products nurtures the persistent interest in spider silk. Suggested applications include different kinds of wearables¹² such as space suits¹³, as durable components in robotics¹⁴, other high-end textiles^{15,16}, and as biomaterials for medical devices^{17–21}. This wide range of applications is attributed to the distinctive property portfolio of spider silk, which combines strength and extensibility, with biocompatibility and biodegradability^{22–24}.

An artificial spider silk fiber intended for commercial applications must display reproducible mechanical properties. The key to gaining control of the fiber's mechanical properties may lie in the understanding of how these are influenced by different spinning conditions. Previous studies have revealed that laboratory-drawn natural spider silk reeled at high speeds displays a high initial Young's modulus and toughness modulus but fractures at low strain^{25,26}. The influence of the spinning conditions on the mechanical properties has also been investigated for fibers obtained from wet-spun recombinant spidroins produced under denaturing conditions. In this process, lyophilized spidroins are first solubilized with hexafluoroisopropanol (HFIP) or trifluoroacetic acid (TFA), followed by extrusion of the concentrated spidroin solution (dope) into a coagulation bath consisting of methanol, isopropanol, or ethanol^{5,10,27,28}. Conditions found to influence the properties of these wet-spun fibers were the chemical composition of the coagulation bath and post-spin stretching^{28,29}. However, since different academic groups most often use custom-made spinning devices and unique spidroin construct(s), and since only a few fibers and conditions are tested in each study, it is difficult to draw general conclusions from the literature on how different spinning conditions impact the mechanical properties of the fibers. The mini-spidroin NT2RepCT with a molecular weight of 33 kDa consists of an N-terminal (NT)³⁰ and C-terminal (CT)³¹ domain, flanking a MaSp1 repetitive region from *Euprosthenois australis* that features two poly alanine blocks³². NT2RepCT is expressed and purified as a water-soluble protein in which the terminal domains are natively folded and functional. In addition, the protein is soluble up to a concentration of 500 mg/mL under conditions that reflect those in the gland lumen (ambient temperatures and

in aqueous buffers at pH 8), which allows NT2RepCT to be spun into fibers using aqueous buffers and a lowered pH combined with shear forces. The production and spinning process herein referred to as a biomimetic spinning process, is substantially different from how artificial spider silk is usually made in that it requires no use of denaturants or organic solvents for solubilization of expressed proteins or fiber spinning². A recent study shows that NT2RepCT can be produced at yields that are compatible with those required for developing a commercial fiber³³. However, NT2RepCT fibers studied in the literature have variable mechanical properties, probably depending on the precise conditions used for spinning (Supplementary Table 1)^{32–36}. In most of these studies, spinning was performed by extruding a highly concentrated (300 mg/mL) NT2RepCT solution (dope) through a tapered glass capillary (tip diameter ~30 μm) into a buffer containing 750 mM acetate (sodium acetate and acetic acid), pH 5, and 200 mM NaCl. In other studies, NT2RepCT fibers were spun using a coaxial needle (straining-flow spinning)³⁴ instead of a glass capillary or were subjected to post-spin incubation in the spinning buffer for several hours before collection³⁵. Another important factor that could influence the mechanical properties of the NT2RepCT fibers is the reeling speed applied during fiber collection, which has not been reported or controlled, except in Schmuck et al.³³.

Hence, a thorough and systematic investigation and optimization of the spinning parameters that influence the properties of the fibers are essential for the continued development of biomimetic artificial spider silk fibers³⁴. In this study we investigate the influence of dope concentration, dope flow rate, the diameter of the capillary opening, humidity, presence of NaCl, reeling speed, buffer composition/temperature, and post-spin stretching to pinpoint the parameters that influence the fibers' mechanical properties (Fig. 1).

Results and discussion

Impact of capillary tip diameter, ionic strength of spinning buffer, dope concentration, flow rate, and relative humidity.

The recently developed production protocol for obtaining NT2RepCT³³ results in unprecedented yields, which made it possible for us to perform a detailed investigation of how a large panel of different spinning parameters affects the mechanical properties of artificial spider silk fibers spun from this protein (Fig. 1). First, we examined the influence of the capillary size on the mechanical properties of biomimetically spun NT2RepCT fibers (Fig. 2. See also Supplementary Table 2 for a summary of all the spinning parameters used in this study). NT2RepCT concentrated to 300 mg/ml was extruded through glass capillaries

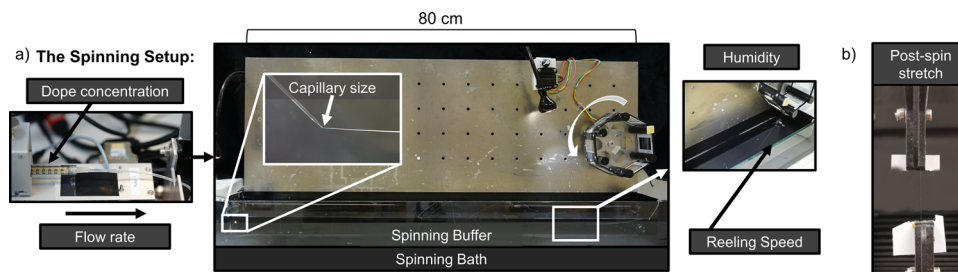


Fig. 1 A custom-made spinning setup for manufacturing biomimetic artificial spider silk with the parameters investigated herein highlighted. **a** A highly concentrated aqueous solution (dope) of the minispidroin NT2RepCT is pumped from a syringe through polyethylene tubing and a glass capillary with a tapered tip into the spinning bath containing an aqueous buffer. At the end of the spinning bath, the fibers are collected on a rotating wheel. Parameters investigated are: 1. Dope concentration (150–450 mg/mL); 2. Flow rate (10–35 μL/min); 3. Capillary size (opening diameter 28–99 μm); 4. Relative humidity (30–85%); 5. The reeling speed (9–69 cm/s); 6. Buffer strength, type, and pH (250–1000 mM acetate/succinate/citrate/citrate-phosphate buffer, pH 4–5). **b** The effect of post-spin stretching was investigated by stretching fibers to defined lengths using a tensile tester.

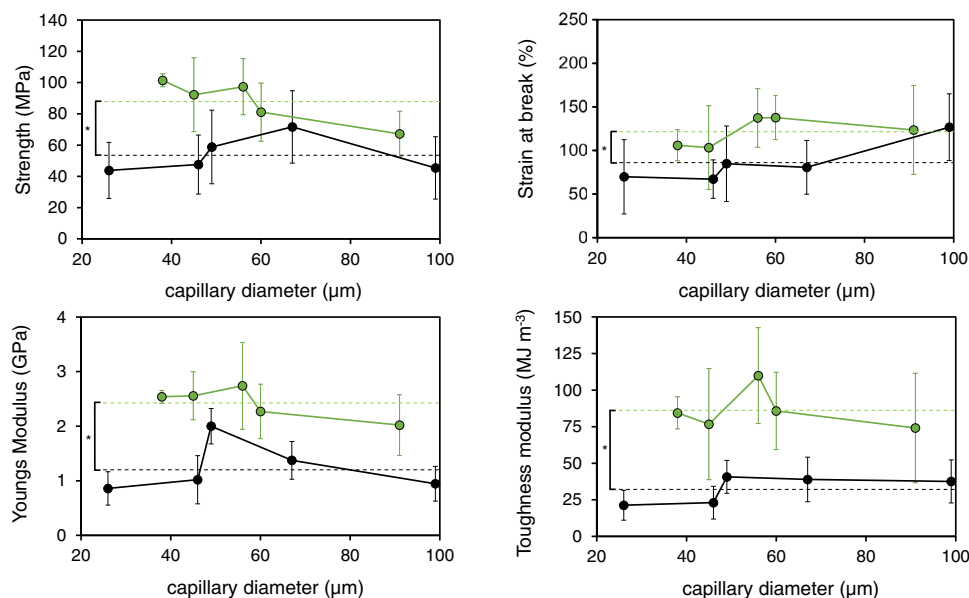


Fig. 2 Impact of capillary tip diameter on the mechanical properties of artificial NT2RepCT silk fibers. Capillaries with six different tip diameters were tested with and without NaCl in the spinning buffer, respectively. The black line connects the data points obtained when a 750 mM acetate (Na) spinning buffer containing 200 mM NaCl was used. The green line represents data points that were obtained with a 750 mM acetate (Na) spinning buffer without NaCl. Each data point represents the average of $n \geq 10$ measurements, with error bars showing \pm one standard deviation. The corresponding stress-strain curves are shown in Supplementary Fig. 1. The dashed lines in Fig. 2 show the average of all data points for the spinning buffer with NaCl (black) or without NaCl (green). Stars indicate a significant difference ($p < 0.01$). Detailed spinning parameters for this experiment are found in Supplementary Table 2.

with an opening in the range from 26 to 99 μm , into a 0.75 M acetate buffer (Na) at pH 5, containing 200 mM NaCl (Fig. 2, black line). These conditions were chosen as a reference since they are comparable to the conditions used for spinning NT2RepCT in earlier work (Supplementary Table 1). The reeling speed was kept constant by collecting the fibers on a rotating wheel at the end of the 80 cm long spinning bath at 29 cm/s. Capillary openings smaller than 50 μm produced fibers with a strain at break of $\sim 70\%$ and strength between 44–59 MPa. Larger capillary openings ($\geq 67 \mu\text{m}$) produced fibers with a strain at break up to 127% and a strength reaching 45–71 MPa. Despite the large size difference in capillary orifice diameters, the fibers produced were rather consistent with respect to strength and the strain at break.

To assess how the ionic strength of the buffer influences the mechanical properties of the mature fibers, the spinning dope was extruded into a spinning buffer without NaCl (0.75 M acetate (Na) at pH 5), using capillaries between 38 and 91 μm . A comparison of the mechanical properties of the fibers spun with and without NaCl in the spinning buffer indeed shows that there is a significant difference (Fig. 2). A toughness modulus of 75 MJ/m^3 to 110 MJ/m^3 was achieved with a spinning buffer without NaCl, while when NaCl was included, the toughness values for fibers spun with all capillary tip sizes were lower than 41 MJ/m^3 . The higher toughness of fibers spun without NaCl in the spinning buffer results from an increase in both strength and strain at break.

Results from both spinning buffer compositions showed a trend of increased fiber diameter (Supplementary Fig. 2) and decreased strength (Fig. 2, green line) with increased capillary orifice size. The best fibers (referring to the toughness modulus) were obtained with a capillary opening of 56 μm which reached a toughness modulus of 110 MJ/m^3 (Fig. 2). Thus, subsequent experiments were conducted with capillaries that had an opening size at the tip of $60 \pm 15 \mu\text{m}$, unless otherwise stated. Moreover, based on these results, subsequent spins were performed without NaCl.

Next, we examined if the protein concentration of the dope influences the mechanical properties. Again, a reeling speed of 29 cm/s was used to collect the fibers after the spinning dope with a protein concentration of 100 to 300 mg/ml was extruded through a glass capillary with a tip diameter between 50 to 70 μm , but up to 100 μm for more concentrated samples. Larger capillary openings were unavoidable as the increased viscosity of highly concentrated samples made it difficult to extrude the spinning dope. An optimum with respect to both strength and strain at break was found for dope concentrations between 250 and 350 mg/mL, while concentrations $< 250 \text{ mg/mL}$ or $> 350 \text{ mg/mL}$ gave fibers with a decreased strength and strain (Fig. 3, left column). When a spinning dope with a concentration of 100 mg/mL was used, fiber collection was not possible, and at 450 mg/mL, the fibers were extremely brittle. Even though fibers spun from 350 mg/mL exhibited the highest toughness so far (115 MJ/m^3), the standard deviation of $\pm 44\%$ is particularly large, and therefore we continued to spin using a dope concentration of 300 mg/mL.

Next, the effect on the mechanical properties of the rate of dope extrusion into the spinning buffer was investigated (Fig. 3, middle column). Slower flow rates (10 & 17 $\mu\text{L}/\text{min}$) resulted in fibers with a strength of 80–100 MPa, whereas fast flow rates (35 $\mu\text{L}/\text{min}$) gave fibers with a lower strength (65–70 MPa) and strain at break. Also, fibers spun using higher flow rates (25 and 35 $\mu\text{L}/\text{min}$), resulted in thicker fibers (Supplementary Fig. 3). Thus, thick fibers were apparently associated with reduced mechanical properties, which is a phenomenon we have observed before and could be caused by a less aligned internal molecular structure³⁷ or by an increased risk of having defects³⁸. It should also be noted that the shear stress in the capillary is not solely correlated to the extrusion rate of the dope, but also to the type of the fluid. Newtonian fluids (whose viscosity does not depend on the shear rate) experience higher shear stresses the higher the shear rates are, inducing more orientation in the protein chains. This is not valid for non-Newtonian fluids, such

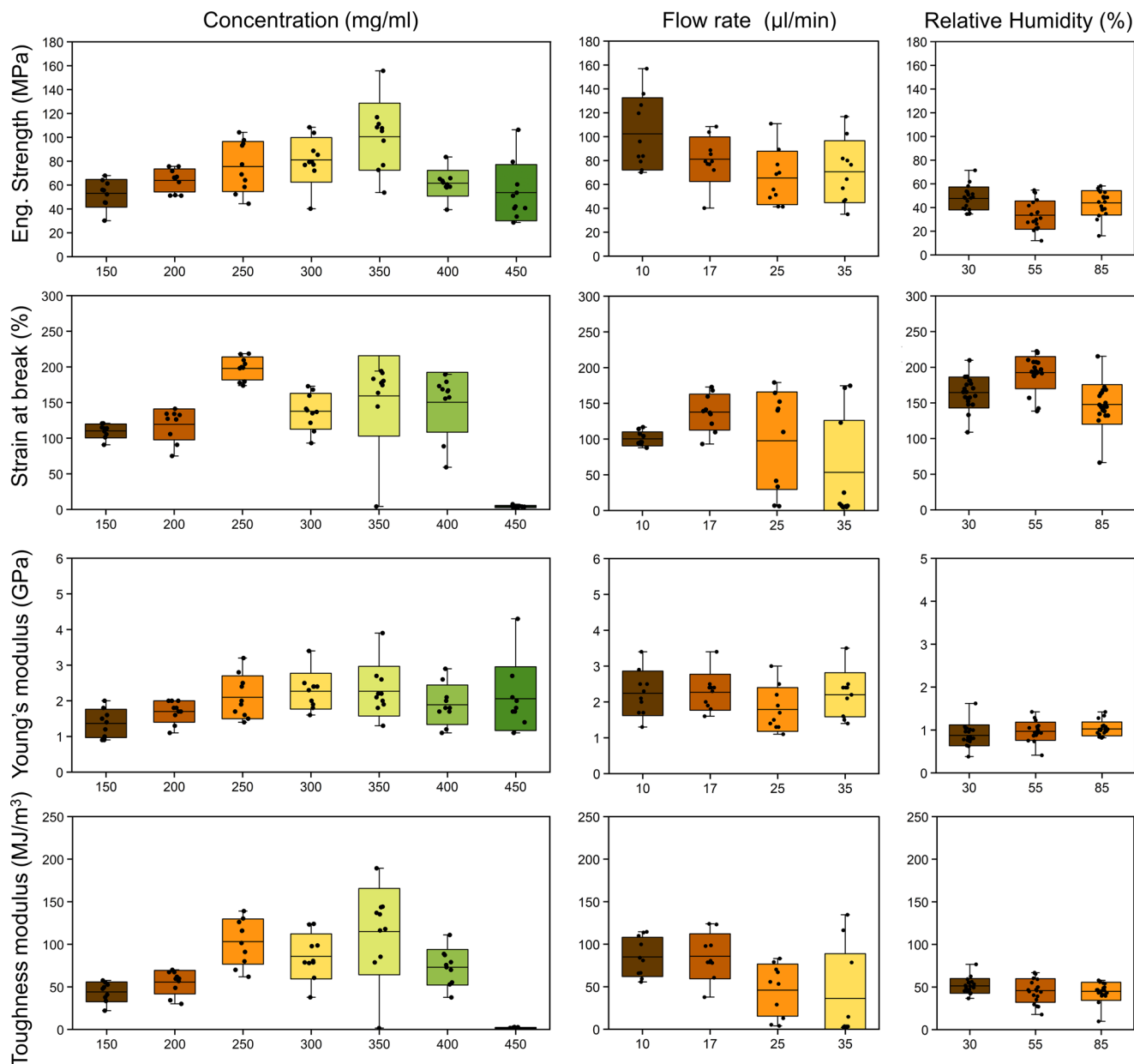


Fig. 3 Influence of the protein concentration, the flow rate, and the relative humidity during the spinning process on the mechanical properties of NT2RepCT fibers. The fibers were obtained by extrusion of a concentrated NT2RepCT solution into 0.75 M acetate pH (5) buffer, using a reeling speed of 29 cm/s for fiber collection. Each point represents one measurement, whiskers indicate the minimal and the maximal value, the boxes show \pm one standard deviation and the horizontal line in the middle of the boxes represents the mean value. The corresponding stress-strain curves are shown in Supplementary Figs. 4 and 5. Left column: Impact of the protein concentration in the spinning dope on the mechanical properties of NT2RepCT fibers. Middle column: Impact of the flow rate of the spinning dope extruded into the spinning buffer on the mechanical properties of NT2RepCT fibers. Right column: Impact of the humidity during spinning on the mechanical properties of NT2RepCT fibers. Detailed spinning parameters for this experiment are found in Supplementary Table 2. Representative SEM images of fibers spun with different dope concentrations are shown in Supplementary Fig. 17.

as the NT2RepCT spinning dope, for which the viscosity is decreased at high shear rates³⁹, which complicates the relationship between flow rate and shear stress. Therefore, increasing the dope flow rate may not have a significant effect on the shear stress and the molecular alignment, which could be why an increase of the flow rate from the previous standard of 17 μ L/min did not improve the strength and strain. Thus 17 μ L/min was used as the flow rate of choice throughout the remaining work.

Another important parameter that needs to be addressed is the effect of the relative humidity on the mechanical properties

of artificial silk fibers. In a previous study by our group, we found that the strength is decreased and the strain is increased if the NT2RepCT fiber is exposed to a relative humidity larger than 50–55% during tensile testing³⁶. Considering this, it is also possible that the fibers are influenced by differences in relative humidity during the spinning process and therefore we evaluated the impact of spinning at a relative humidity between 30% to 85% (Fig. 3, left column). From the data obtained, no major changes in the mechanical properties of the fibers could be observed, which is in line with what has been observed for native spider silk⁴⁰.

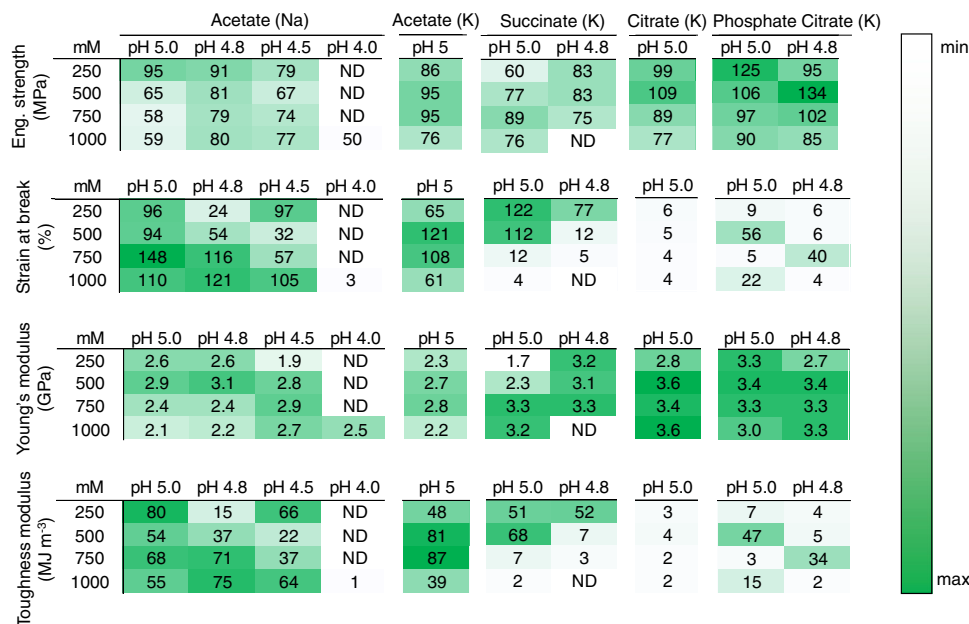


Fig. 4 Mechanical properties of NT2RepCT fibers spun with a variety of buffers. For better orientation, the values were colored according to a gradient from white (low) to (high (dark green)). ND (not defined) designates buffers that could not produce enough fibers for tensile testing. The values shown here represent the average of $n \geq 10$ measurement. The same table but with \pm one standard deviation is shown in Supplementary Fig. 7. The corresponding stress-strain curves are shown in Supplementary Figs. 8–12. Details regarding other spinning parameters of this experiment are found in Supplementary Table 2.

Influence of the spinning buffer. The lock and trigger hypothesis for native spider silk formation states that the decreased pH observed along the silk gland leads to NT dimerization (locking the spidroins together) and CT unfolding³, which in turn triggers the formation of β -sheet polymers of the repetitive region. Since the CT remains folded in NT2RepCT fibers spun using acetate buffer at pH 5⁴¹, in an attempt to make the fibers stronger, we speculated that decreasing the pH in the spinning buffer (below 5) could facilitate unfolding of CT. Spinning of NT2RepCT at different pH values was tested by Andersson et al.³², where a spinnability between pH 5.5 and 3 is reported. However, the mechanical properties of the fibers spun at other pH values than 5 were not determined. Here, we evaluate the mechanical properties of fibers spun at different pH values, also using different buffer strengths (between 250 to 1000 mM) and different buffer types (acetate, succinate, citrate, and citrate phosphate, see Fig. 4). In total, we attempted to produce fibers from NT2RepCT dopes using 40 different spinning bath buffers. To help us get an overview and decide which conditions were favorable, we initially categorized the spinning process as being continuous (fiber collection without interruption), discontinuous (frequent interruption as the fiber would break during collection after less than 10 s, making it necessary to guide the fiber once more from the capillary through the spinning bath to the collection wheel), or not possible to collect a fiber (the fiber was too fragile and would either disintegrate or break during translocation through the spinning bath). Using the acetate (Na) buffer, but decreasing the pH made it more and more difficult to attain a continuous spinning process (Supplementary Fig. 6). At pH 4, the wet fiber was extremely fragile, which made it impossible to collect enough fiber for tensile testing, except at an acetate concentration of 1000 mM when fiber collection was discontinuous but could be maintained for a few seconds. Discontinuous spinning was also observed for pH 4.5 using low acetate concentrations of 250 and 500 mM. Tensile testing of fibers produced using the entire acetate (Na) matrix (250–1000 mM and pH 4–5) showed that the fiber strength was rather consistent (58–95 MPa) except for fibers

obtained at pH 4 which had both strain at break and strength values that were inferior to all the other fibers (Figs. 4 and Supplementary Fig. S7). On the other hand, the strain at break of the fibers spun using the different acetate (Na) buffers varied substantially. Higher extensibility was obtained for fibers spun using high acetate (Na) concentrations (≥ 750 mM) if the pH was ≥ 4.5 (Fig. 4). One exception was fibers spun using 250 mM acetate (Na) at pH 4.5 which showed high extensibility but also very large variability (Supplementary Fig. 7). Taken together, our results indicate that the optimal pH value of the spinning buffer is 5, but that the acetate concentration does not have a substantial effect on the mechanical properties of the fibers. Lowering the pH in the spinning buffer to < 5 does not result in stronger fibers, in contrast to what could be speculated based on the functions of the CT.

Natural silk-spinning involves a gradually decreasing pH but also relies on changes in ion concentrations along the spinning duct^{42,43}. In particular, the concentrations of the chaotropic ions Na^+ and Cl^- are lowered, while the concentrations of the kosmotropic ions PO_4^{3-} and SO_4^{2-} are increased⁴³. Na^+ has been suggested to weaken intra- and intermolecular interactions of the repetitive domains and prevent their transition into β -sheet conformation, while kosmotropic ions would have the opposite effect⁴⁴. In line with this, we replaced Na^+ with K^+ in the spinning buffer by preparing an acetate (K) buffer at pH 5. Using buffer concentrations of 250, 500, 750, and 1000 mM, respectively, we produced fibers with a strain at break of up to 121% and tensile strength of 76–95 MPa which is similar to the tensile properties obtained using acetate (Na) (Figs. 2 and 3). This means that in our spinning system, there is no advantage to using K^+ over Na^+ ions in the spinning buffer. The lack of detectable effects of replacing K^+ for Na^+ in the spinning bath could be a consequence of that we introduce an abrupt change in conditions when the dope is extruded into the spinning buffer rather than mimicking the gradual change in ion concentration in the spider's gland.

Finally, we also investigated if alterations in the buffering system would modulate the mechanical properties. First, we

tested divalent succinate buffers, which resulted in fibers with a strength that was comparable to fibers spun in acetate buffers (Fig. 4). At high succinate concentrations, there was a significant decrease in strain. Lowering the pH of the succinate buffers to 4.8 impair the strain relative to pH 5 and made it impossible to spin at 1000 mM. The use of citrate as a spinning buffer has previously been shown to yield extensible fibers when spinning regenerated silkworm fibroins, e.g. Chen et al. produced fibers with a strength of 76–98 MPa and a strain at break of 40–104%⁴⁵, which is comparable to NT2RepCT fibers (Fig. 2). In our hands, a citrate buffer and a phosphate-citrate spinning buffer, respectively, resulted in stronger fibers (strength up to 134 MPa) with a higher Young's modulus (up to 3.4 GPa) but with the trade-off of an inferior strain at break (5–56%). Fibers spun with a citrate buffer had a substantially lower toughness than acetate-spun fibers (2–47 MJ/m³). We also lowered the pH to 4.8 in the citrate phosphate buffer, but it did not lead to an improvement of the mechanical properties compared to the citrate phosphate buffer at pH 5 (Fig. 4).

Overall, the choice of the buffering system has a large effect on the mechanical properties of the fibers inasmuch as strength values differ by a factor of 2, strain values differ by a factor of 50, and the toughness modulus can vary up to 2 orders of magnitude between fibers spun under the conditions investigated herein. However, we could not identify any spinning bath buffer composition that improved the mechanical properties of the fibers compared to the acetate buffer (Na), which continued to be the standard for spinning NT2RepCT fibers.

Influence of the reeling speed. Next, we investigated the influence of the reeling speed on the mechanical properties using the 0.75 M acetate buffer (Na), by varying this parameter between 17 cm s⁻¹ and 69 cm s⁻¹, which was in the range that was feasible for continuous spinning. From these experiments two major conclusions became evident. First, higher reeling speeds correlated with stronger fibers. At low reeling speeds (17 cm/s) the strength of the NT2RepCT fibers is lower than 30 MPa, but if the reeling speed is increased the average strength approaches 100 MPa and more (Fig. 5). The fiber with the highest strength (114 MPa) was obtained at 58 cm s⁻¹. This demonstrates the importance of always reporting the reeling speed when spinning artificial silk fibers and could be an explanation for the large deviations of the mechanical properties found in earlier studies (Supplementary Table 1). Second, with increasing reeling speed there is a trend toward lower strain at break (Fig. 5), a correlation which was also reported in the literature for native silk^{43,46}, but since there is an opposite trend for the tensile strength, the toughness values are fairly constant for reeling speeds ≥ 29 cm/s and ≤ 58 cm/s. Again, excluding NaCl from the spinning buffer in this set-up results in fibers with better mechanical properties (Supplementary Fig. 14).

The fibers with the highest toughness modulus in this experimental series were produced at 29 cm/s, reaching 89 MJ/m³ (Fig. 5), but they also displayed a large variability, which is typical for silk materials⁴⁷. Because of this, we decided to increase the sample sizes for fibers spun at 29 cm s⁻¹ and 58 cm s⁻¹ (highest toughness and highest strength, respectively). 79 individual NT2RepCT fibers that were spun at 29 cm s⁻¹ on six different occasions and 89 fibers spun at 58 cm s⁻¹ on eight different occasions were tested. The mechanical properties of all tested fibers produced under these two conditions are found in Fig. 6. Fibers spun at 58 cm s⁻¹ exhibited a significantly higher strength (110 MPa compared to 75 MPa at 29 cm s⁻¹), but the strain at break was as expected significantly reduced (113% compared to 151% at 29 cm s⁻¹).

There was no statistically significant difference in fiber toughness between the two groups (90 MJ/m³ and 80 MJ/m³, respectively). The Young's modulus for fibers produced at 29 cm s⁻¹ was 1.9 GPa while the fibers spun at 58 cm s⁻¹ were stiffer with a Young's modulus of 2.2 GPa. As expected, a higher reeling speed led to smaller fiber diameters (10.5 μ m at 29 cm s⁻¹ compared to 8.8 μ m at 59 cm/s) (Fig. 6). A recent study reported that an artificial spider silk fiber's strength is positively correlated to its birefringence under polarized light and both parameters can be increased by increased reeling speeds³⁷. Using brightfield microscopy, we could not detect any morphological difference as both fiber types (spun at 29 cm s⁻¹ and 58 cm s⁻¹, respectively) seemed rather uniform in shape (Fig. 7). However, an investigation of the fibers using polarized light microscopy, revealed that the birefringence of fibers reeled at 59 cm/s is substantially higher compared to fibers reeled at 29 cm/s (Fig. 7). This suggests, that the internal molecular structure is indeed affected by the reeling speed, which is in agreement with what has been found for native silk⁴⁶.

Temperature of the spinning buffer. Another strategy to facilitate the unfolding of CT could be to increase the temperature, as suggested in a previous report⁴². To test this we spun fibers in a spinning buffer that held a temperature of 22, 34, 42, and 46 °C, respectively. Continuous spinning at a reeling speed of 59 cm/s was possible up to ~ 42 °C. At 46 °C spinning was discontinuous. Spinning at temperatures higher than 46 °C was impossible since the spinning dope solidified⁴⁸ in the tip of the capillary as soon as it was immersed into the buffer, thus blocking the outlet. With respect to the mechanical properties of the fibers spun at higher temperatures compared to the standard temperature (22 °C), the strength was decreased, and the fiber-to-fiber variation increased substantially which indicates suboptimal spinning conditions (Fig. 8). Furthermore, accelerating the drying speed of the freshly reeled fibers by placing an infrared light source in the vicinity of the collection wheel has had no significant effect on the mechanical properties (Supplementary Fig. 19).

Post spin stretching. Post-spin stretching is a commonly used method that increases the strength of natural and synthetic fibers⁴⁹, and is a fundamental element in the industrial production of fibers^{50,51}. This is also true for artificial silk fibers⁵² which, after extrusion of the dope into a methanol or isopropanol coagulation bath, often are manually stretched 4–6 times of their original length before they are tensile tested^{5,9,10,53}. Detailed quantification of the influence of post-spin stretching could provide useful information to maximize the strength^{28,52}, as has been shown e.g. for a fiber made from regenerated silk fibroin that gained an increased strength of up to 80% with a 2-fold drawing ratio^{45,54,55}. There are no reports of post-spin stretched NT2RepCT fibers, as all the fibers described thus far refer to as-spun fibers (Supplementary Table 2). In this study, we attempted for the first time to quantify the effect of post-spin stretching NT2RepCT fibers. For this purpose, fibers spun at 58 cm s⁻¹ were mounted in a tensile tester and stretched 20%, 40%, 60%, and 80% (Fig. 9). Then the fibers were recovered and allowed to relax before they were finally tensile tested. As anticipated, we found a positive correlation between the draw ratio and strength, but also a negative correlation between the draw ratio and strain at break, which is a common effect of post-spin stretching. The highest draw ratio investigated here (80%) increased the strength significantly to 261 MPa, which corresponds to an improvement of 90%, which is the highest reported strength for a biomimetically spun fiber from NT2RepCT (Supplementary Table 1). Stretching the fibers by 80% also increased the Young's modulus to 4.8 GPa,

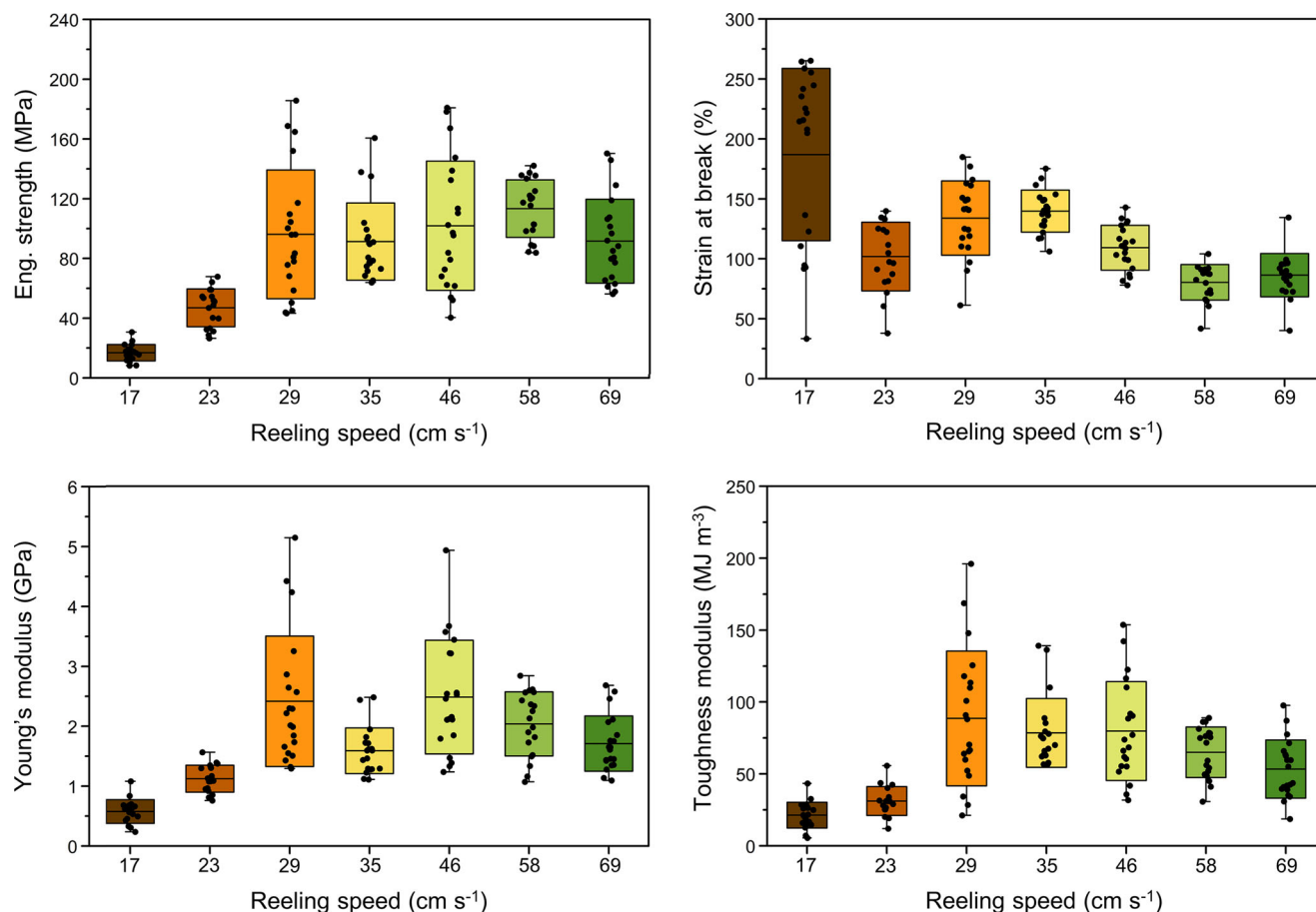


Fig. 5 Dependence of the mechanical properties of NT2RepCT fibers on the reeling speed. A 750 mM acetate (Na) buffer at pH 5 was used as spinning bath. This figure depicts the data as a box plot, where each data point represents one measurement, whiskers indicate the minimal and the maximal value, the boxes show \pm one standard deviation, and the horizontal line in the middle of the boxes represents the mean value of $n \geq 10$. The corresponding stress-strain curves are shown in Supplementary Fig. 13. Other spinning parameters associated with this experiment are found in Supplementary Table 2.

which corresponds to a doubling of the stiffness compared to unstretched fibers. The best fiber in terms of toughness modulus was obtained by stretching the fiber 20%, which increased the toughness modulus to 129 MJ/m^3 and means that these NT2RepCT fibers are six times tougher than Nylon and three times tougher than Kevlar^{33,56,57}. If the fiber is stretched by 80%, the toughness modulus of NT2RepCT fibers is decreased to 68 MJ/m^3 , which is still substantially tougher than Nylon and Kevlar.

Figure 10 displays an overview of the impact of some of the different spinning conditions investigated herein on fiber mechanical properties. The spinning conditions affect the fiber properties greatly, as evidenced by the 10-fold difference between the lowest and highest tensile strength and a 150-fold difference between the lowest and highest toughness modulus. The plot reveals that a monovalent acetate buffer, but without NaCl, is optimal to obtain fibers with a high average toughness modulus. Furthermore, an important factor for obtaining strong fibers is to reel the fresh fiber at high speeds, and in addition apply post-spin stretching, which gives a clear indication that these parameters should be quantified and reported in future studies. Overall, this work provides important and valuable information for future developments of biomimetic artificial silk fibers, but it is plausible that the parameters investigated herein have other effects on the mechanical properties of fibers spun from spidroins with a different primary structure (e.g. that have repetitive regions derived from other types of spidroins), which should be

investigated in future studies. In addition, our results may not be directly translatable to processes that use protein denaturation and aggregation (by spinning into e.g. isopropanol) to form artificial spider silk fibers.

Conclusion

The recent development of a protocol that allows expression of NT2RepCT with a bioreactor at yields surpassing 20 g/L allowed us to herein screen a large number of different spinning conditions and tensile test more than 1000 fibers. Our results show that the optimized spinning protocol is insensitive to minor alterations in protein concentration of the spinning dope (between 250 and 350 mg/mL), the diameter of the capillary used for extrusion (30 – $70 \mu\text{m}$), the buffer concentration (250 – 1000 mM at pH 5), as well as the relative humidity during the spinning process (30 – 85%). At the same time higher flow rates ($>17 \mu\text{l/min}$), concentrations of $>350 \text{ mg/ml}$ or $<250 \text{ mg/ml}$, and the addition of NaCl to the spinning buffer is accompanied by a negative effect on the fiber mechanical properties. A pH <4.8 in the spinning bath made the spinning process discontinuous. Replacement of the acetate spinning bath buffer with other buffers made the artificial silk fibers stronger at the expense of a substantially decreased extensibility. Stretching of the fiber, either by increasing reeling speed or by post-spin stretching, was the single most important factor that improved the mechanical tensile strength of the fiber. The toughness of the fibers spun under the most optimal conditions we identified (129 MJ/m^3) is more than three

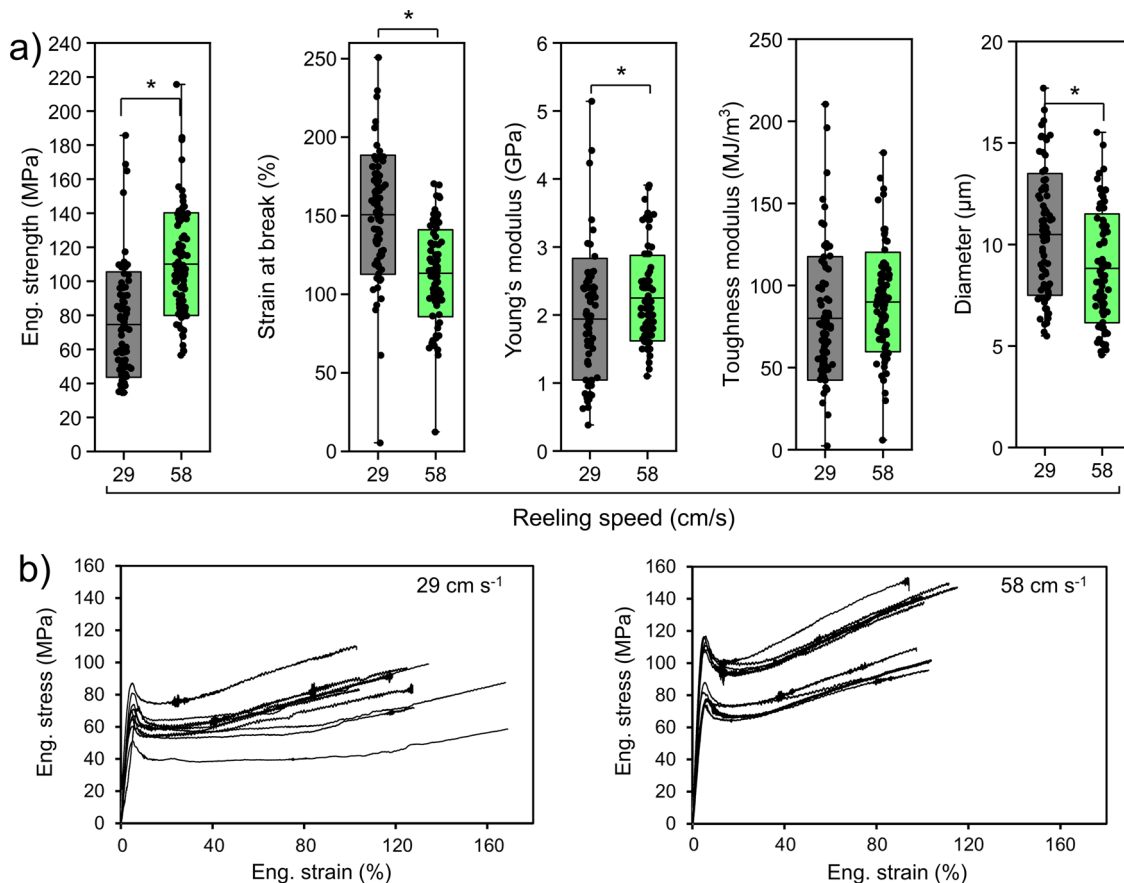


Fig. 6 The mechanical properties of NT2RepCT fibers spun at 29 and 58 cm/s at several different occasions. **a** 79 fibers spun at 29cm/s at 6 different occasions, and 89 fibers spun at 59 cm/s at 8 different occasions were tensile tested. Whiskers indicate the minimal and the maximal value, the boxes show \pm one standard deviation and the horizontal line in the middle of the boxes represents the mean value. A significant difference ($p < 0.05$) is indicated with stars. The mean values for each individual spin highlighting the spin-to-spin variation are shown in Supplementary Fig. 15. **b** Representative stress-strain curves of both fiber types spun at 29 cm/s and 59 cm/s are shown. Additional spinning parameters relevant to this experiment are found in Supplementary Table 2.

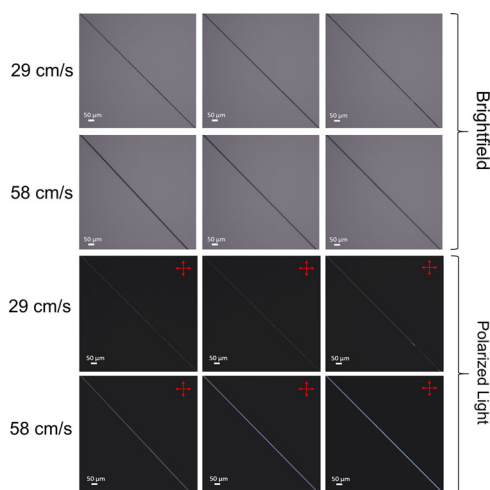


Fig. 7 Representative brightfield and polarized light microscopy images of NT2RepCT fibers. Three different fibers obtained at a reeling speed of 29 and 58 cm/s are shown. The red double arrows represent the direction of the polarizers. Representative SEM images of these fibers and fibers obtained in different conditions are shown in Supplementary Figs. 16 and 17.

times higher than man-made high-performance fibers like Kevlar and Nylon-6.

Methods

Biomimetic spinning. The mini-spidroins NT2RepCT with a molecular weight of 33 kDa³² were produced with an expression and purification protocol described earlier³³. After purification, the minispidroins were concentrated to 300 mg/mL (the spinning dope) with an Amicon Ultra-15 centrifugal filter unit (Merck-Millipore) equipped with an ultracel-10 membrane (10 kDa cutoff) at 4000 \times g and 4 °C. The spinning dope was then transferred to a 1 mL syringe with a luer lock tip (BD, Franklin Lakes, NJ, USA). Biomimetic spinning was essentially performed as suggested by Greco et al.³⁵, with some modifications. The syringe filled with the spinning dope was mounted in a neMESYS low pressure (290 N) syringe pump (Cetoni, Korbussen, Germany) and connected to a 27 G blunt end steel needle (B. Braun, Melsungen, Germany), which was connected to a pulled glass capillary by using a serial tubing connection. Polyethylene tubing (BD Intramedic, Franklin Lakes, NJ, USA) with an outer diameter (O.D.) of 1.09 mm and inner diameter (I.D.) of 0.38 mm was used to encase the needle before it was inserted ~1 cm into the larger polyethylene tubing with an O.D. of 1.65 mm and an I.D. of 0.76 mm. The glass capillary (G1 Narishige, Tokyo, Japan) with an O.D. of 1.0 mm and I.D. of 0.6 mm was inserted into the end of the larger polyethylene tubing. Before insertion, the glass capillary was heated and pulled using a Micro Electrode Puller (Stoelting Co. 51217, Wood Dale, IL, USA). To obtain a tapered tip with an orifice diameter of <100 µm the capillaries were cut by hand and investigated under light microscopy at 10 \times magnification to remove capillaries that were damaged and to determine the diameter of the tip opening. After the connection between the syringe and the glass capillary was established, the spinning dope was extruded through the capillary with a flow rate of 17 µl/min into the spinning bath containing 4 L of a 750 mM acetate (Na) buffer at pH 5. The distance the fiber traveled

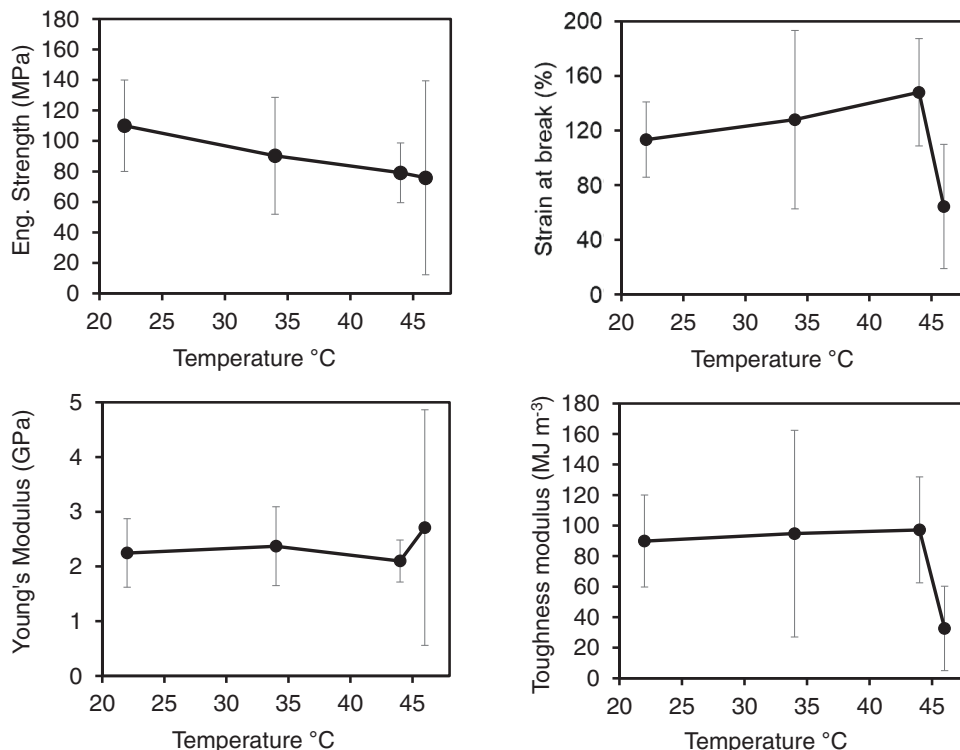


Fig. 8 Tensile properties of NT2RepCT fibers as a function of the temperature of the spinning buffer. All fibers were collected at a reeling speed of 58 cm/s. The reference fibers at 22 °C is the grand average of all fibers spun at 58 cm/s, as shown in Fig. 6. Each data points represents the average of $n \geq 10$ measurements, with error bars \pm one standard deviation. The corresponding stress-strain curves are shown in Supplementary Fig. 18. Other parameters relevant for this spinning experiment are found in Supplementary Table 2.

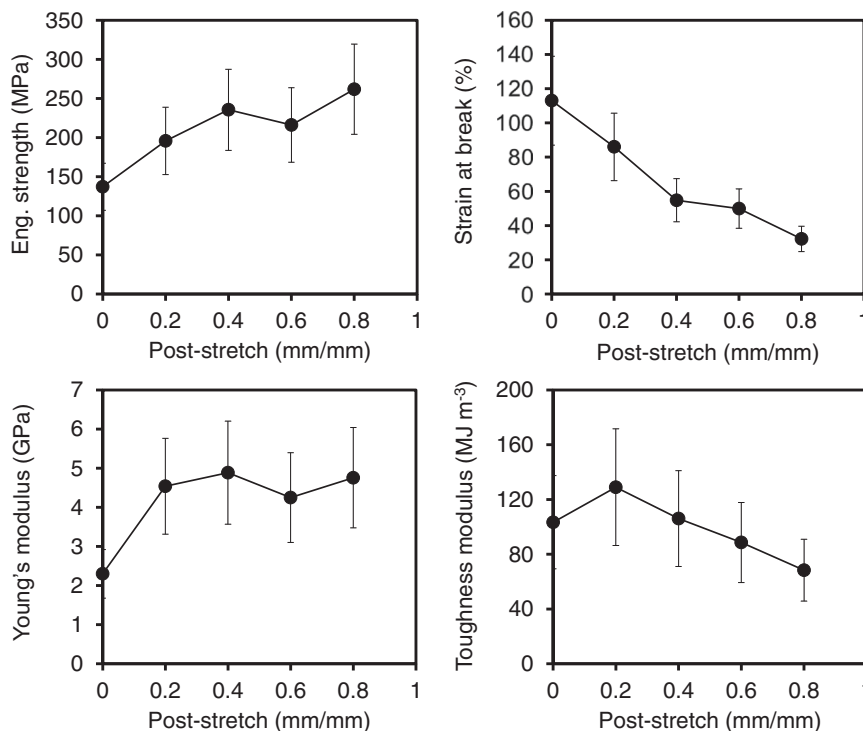


Fig. 9 Influence of post-spin stretching on the mechanical properties of as-spun NT2RepCT fibers. The NT2RepCT fibers were stretched by either 0% ($n = 20$), 20% ($n = 8$), 40% ($n = 8$), 60% ($n = 6$), or 80% ($n = 7$) their original length, with a tensile tester. After this treatment, the fibers were recovered, the diameter was determined before the fibers were finally tensile tested. Each data point represents the average with error bars indicating \pm one standard deviation. The corresponding stress-strain curves are shown in Supplementary Fig. 20.

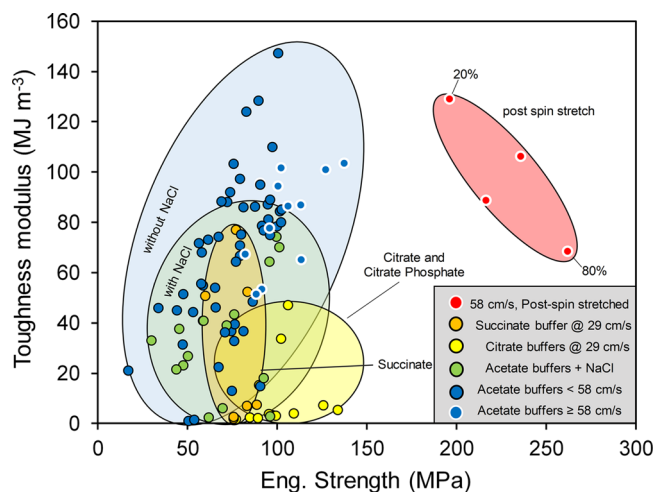


Fig. 10 An Ashby plot featuring the engineering strength and toughness modulus of all fibers tested in this study. In total fibers were obtained in 103 independent spinning occasions, where each point in the diagram represents the average stress and strain of $n \geq 10$ fibers spun under a specific condition, except for fibers which were post spin stretched ($n \geq 6$).

through the spinning bath was 80 cm prior to collection using a wheel with a circumference of 35 cm using a reeling speed of 58 cm/s (100 rpm). Usually, continuous fiber collection was performed for 60–90 seconds until enough fibers for tensile testing and other characterizations were collected.

Biomimetic spinning with conditions that deviate from the standard protocol.

When assessing different spinning parameters, the protocol described above was implemented but with the deviations listed below. A detailed summary of the different experimental conditions for each set of experiments is found in Supplementary Table 2.

Diameter of capillary tip. Capillaries with tip orifice diameters in the range of 26 and 99 μm (as indicated in Fig. 2) were used for extrusion of the spinning dope. In this setup, the dope was extruded into the 750 mM acetate (Na) buffer at pH 5 either with or without NaCl (200 mM). The acetate buffer with NaCl is a standard in the literature when spinning NT2RepCT^{32–36,58}.

Concentration. The NT2RepCT minispidroins were concentrated to generate spinning dopes at concentrations ranging from 100 mg/mL to 450 mg/mL, in steps of 50 mg/mL (indicated in Fig. 3). For each concentration, the spinning dope was carefully mixed, and the protein concentration was measured in triplicates, by measuring the absorbance at 280 nm of a 300-fold diluted sample and using the sequence-specific extinction coefficient ($18,910 \text{ M}^{-1} \text{ cm}^{-1}$) to calculate the concentration.

Flow rate. A neMESYS low pressure (290 N) syringe pump (Cetoni, Korbußen, Germany) was used to extrude the spinning dope (300 mg/mL) into the 750 mM acetate buffer, pH 5 at 10, 17, 25, and 35 $\mu\text{l}/\text{min}$.

Humidity. To control the humidity, the spinning machine including all its components and the syringe pump was placed in a plastic greenhouse tent together with either a humidifier (Homasy HM421A) or a dehumidifier (ProBreeze PB-06) to obtain a local environment with the desired relative humidity. For relative humidities lower than ambient conditions the dehumidifier was set to 30%. Spinning of NT2RepCT was initiated once the relative humidity value was stable and confirmed with a hygrometer. Higher relative humidities of 55% and 80%, respectively, were achieved with a humidifier. After spinning at 30%, 55%, and 85% the collected fibers were incubated on the collection wheel for 10 min before they were recovered.

Buffer composition. To investigate the influence of the spinning buffer on the mechanical properties of the fibers, five different buffer systems were used. The acetate buffer, with its corresponding cation Na^+ , was obtained by mixing 0.33 M acetic acid and 0.67 M Na-acetate to achieve a final acetate concentration of 1 M with a pH of 5. Lower concentrations or pH values were obtained in the same manner. With respect to this buffer, it is important to note the typical spinning buffer reported in the literature is referred to as 500 mM Na-acetate, for instance by Andersson et al.³², which corresponds to a 750 mM acetate buffer considering the amount of acetic acid used to adjust the pH to 5. In this study, to avoid confusion when stating the buffer concentration, we refer to the concentration of the conjugate base and report the corresponding cation in parentheses (for instance Na).

The acetate buffer with the cation K^+ was obtained by preparing a 1 M acetic acid and adjusting the pH to 5 with KOH. Succinate buffer and the citrate buffer with the cation K^+ were prepared by dissolving 1 M succinic acid or citric acid in dH_2O and then adjusting the pH to 5 with KOH. To prepare the phosphate citrate buffer (as an example 1 M), 0.68 M dipotassium hydrogen phosphate was mixed with 0.32 M citric acid to reach a pH of 5. Buffers with different concentrations and pH values were obtained in the same manner.

Reeling speed. The reeling speed for fiber collection was varied between 15–120 rpm, corresponding to 9–69 cm/s. The dope was extruded into a 0.75 M acetate buffer (Na), pH 5, both with and without 200 mM NaCl.

Temperature of the spinning bath. The spinning buffer was heated in a separate beaker and then quickly transferred into the spinning bath. The temperature of the spinning buffer was determined with a thermometer immersed in the spinning bath, a few seconds before spinning was initiated. The temperature of the spinning buffer did not change significantly during the spinning process since enough fibers were collected for tensile testing within 60–90 s.

IR lamp. An PAR38E IR lamp (Philips) with an effect of 150 W was placed at 8 cm or 15 cm from the fiber collection wheel, respectively. After the sample was collected for ~ 1 min, spinning was aborted, but the wheel was allowed to rotate for another 5 minutes to ensure even exposure to the heat. The experiment was performed at a reeling speed of both 29 and 58 cm/s.

Post spin stretching. Freshly spun fibers were mounted on paper frames with a square window of 10×10 mm and mounted in an Instron 5943 tensile tester whereafter the sides of the paper frames were cut. The fibers were then stretched at 20%, 40%, 60%, and 80% with the tensile tester and relaxed for 10 minutes at the pre-determined level of strain. Subsequently, the fibers were removed from the frame and carefully re-mounted on new paper frames with a square window of 10×10 mm and used for tensile testing (see below).

Brightfield and polarized microscopy. Images were collected using a Nikon Eclipse Ts2R-FL inverted microscope equipped with a DFKNME33UX264 5 MP camera and a CFI Plan Fluor DL-10X objective. Image capture was done using the Nikon NIS-Elements BR software. Exposure time was set to 2 ms for bright-field images and 50 ms for polarized microscopy (POM) images. Individual fibers were fixed with double-sided tape to paper frames with a 10 mm gap, placed on microscope glass slides, and oriented 45 degrees relative to the direction of the microscope polarizers prior to capture. For improved visualization, the brightness of the POM micrographs was increased by 50% post-capture after first being saved as a single image using Microsoft PowerPoint. Six consecutive POM images were acquired from three representative fibers spun at 29 cm/s and 59 cm/s, respectively.

Tensile testing. The mechanical properties for each fiber type were determined by tensile testing of 10 to 20 randomly selected fibers from each fiber sample collection⁴⁷. Before tensile testing, each fiber was mounted on a paper frame over a 10×10 mm square window and fixed with double-sided tape. Then, the diameter was determined by light-microscopy at $10\times$ magnification, by averaging the determined diameters (three measurements with Eclipse Net 1.20.0) from three images taken with a Digital Sight DS-5M (Nikon) from randomly selected fiber segments. The cross-sectional area of each fiber was computed using the average diameter of that fiber assuming a circular cross-section, as is custom practice for silk fibers^{5,9,10,33,34,59}. Tensile tests were performed with an Instron 5943 tensile tester at ambient conditions ($19\text{--}21^\circ\text{C}$, $<35\%$ RH) and a strain rate of 6 mm/min, and a 5 N load cell. The engineering strength was computed by dividing the force by the average cross-sectional area for each fiber. The engineering strain was calculated by dividing the fiber displacement by the gauge length. The toughness modulus was obtained by calculating the total area under the stress-strain curve, and the Young's modulus was determined from the slope of the linear elastic part. No outliers were removed from the data.

Statistical analysis. One-way pairwise ANOVA analysis was performed with the support of Matlab[®] with the function `anova1()`. The difference of a specific mechanical property was considered significant between two fiber samples if the two-tailed p-value was lower than 5%.

Scanning electron microscopy. An Emission Field Scanning Electron Microscope (Zeiss Supra-40) was used to investigate the morphology of the fibers. These were placed on aluminum stabs and coated with a Pt/Pd (80:20) alloy utilizing a sputtering machine (Quora Q150). The accelerating voltages were 2.5–5 kV.

Data availability

The datasets generated during and/or analyzed during the current study are available from the corresponding author on reasonable request.

Received: 16 May 2022; Accepted: 13 October 2022;

Published online: 04 November 2022

References

- Esselen, G. J. Production of Silk Fibers. US Patent US1934413 A. (1933).
- Koepfel, A. & Holland, C. Progress and trends in artificial silk spinning: a systematic review. *ACS Biomater. Sci. Eng.* **3**, 226–237 (2017).
- Rising, A. & Johansson, J. Toward spinning artificial spider silk. *Nat. Chem. Biol.* <https://doi.org/10.1038/nchembio.1789> (2015).
- Dobhofer, E., Heidebrecht, A. & Scheibel, T. To spin or not to spin: spider silk fibers and more. *Appl. Microbiol. Biotechnol.* <https://doi.org/10.1007/s00253-015-6948-8> (2015).
- Xia, X. X. et al. Native-sized recombinant spider silk protein produced in metabolically engineered *Escherichia coli* results in a strong fiber. *Proc. Natl. Acad. Sci. USA* **107**, 14059–14063 (2010).
- Debabov, V. G. & Bogush, V. G. Recombinant spidroins as the basis for new materials. *ACS Biomater. Sci. Eng.* **6**, 3745–3761 (2020).
- Hinman, M. B., Jones, J. A. & Lewis, R. V. Synthetic spider silk: a modular fiber. *Trends Biotechnol.* **18**, 374–379 (2000).
- Fahnestock, S. R. & Irwin, S. L. Synthetic spider dragline silk proteins and their production in *Escherichia coli*. *Appl. Microbiol. Biotechnol.* **47**, 23–32 (1997).
- Bowen, C. H. et al. Recombinant spidroins fully replicate primary mechanical properties of natural spider silk. *Biomacromolecules* **19**, 3853–3860 (2018).
- Heidebrecht, A. et al. Biomimetic fibers made of recombinant spidroins with the same toughness as natural spider silk. *Adv. Mater.* **27**, 2189–2194 (2015).
- Rising, A., Widhe, M., Johansson, J. & Hedhammar, M. Spider silk proteins: recent advances in recombinant production, structure-function relationships and biomedical applications. *Cell. Mol. Life Sci.* **68**, 169–184 (2011).
- Blamires, S. J., Spicer, P. T. & Flanagan, P. J. Spider silk biomimetics programs to inform the development of new wearable technologies. *Front. Mater.* <https://doi.org/10.3389/fmats.2020.00029> (2020).
- Weiss, P. et al. Advanced materials for future lunar extravehicular activity space suit. *Adv. Mater. Technol.* <https://doi.org/10.1002/admt.202000028> (2020).
- Pan, L. et al. A supertough electro-tendon based on spider silk composites. *Nat. Commun.* **11**, 1332 (2020).
- Salehi, S. & Scheibel, T. Biomimetic spider silk fibres: from vision to reality. *Biochemist* **40**, 4–7 (2018).
- Lefèvre, T. & Auger, M. Spider silk as a blueprint for greener materials: a review. *Int. Mater. Rev.* **61**, 127–153 (2016).
- Kluge, J. A., Rabotyagova, O., Leisk, G. G. & Kaplan, D. L. Spider silks and their applications. *Trends Biotechnol.* <https://doi.org/10.1016/j.tibtech.2008.02.006> (2008).
- Dellaquila, A. et al. Optimized production of a high-performance hybrid biomaterial: biomaterialized spider silk for bone tissue engineering. *J. Appl. Polym. Sci.* <https://doi.org/10.1002/app.48739> (2020).
- Schacht, K., Vogt, J. & Scheibel, T. Foams made of engineered recombinant spider silk proteins as 3d scaffolds for cell growth. *ACS Biomater. Sci. Eng.* <https://doi.org/10.1021/acsbomaterials.5b00483> (2016).
- Chouhan, D. et al. Recombinant spider silk functionalized silkworm silk matrices as potential bioactive wound dressings and skin grafts. *ACS Appl. Mater. Interfaces* <https://doi.org/10.1021/acsami.8b05853> (2018).
- Bourzac, K. Spiders: Web of intrigue. *Nature* **519**, S4–S6 (2015).
- Radtke, C. et al. Spider silk constructs enhance axonal regeneration and remyelination in long nerve defects in sheep. *PLoS One* **6**, e16990 (2011).
- Agnarsson, I., Kuntner, M. & Blackledge, T. A. Bioprospecting finds the toughest biological material: Extraordinary silk from a giant riverine orb spider. *PLoS One* **5**, 1–8 (2010).
- Greco, G. & Pugno, N. M. Mechanical properties and weibull scaling laws of unknown spider silks. *Molecules* **25**, 2938 (2020).
- Yarger, J. L., Cherry, B. R. & Van Der Vaart, A. Uncovering the structure-function relationship in spider silk. *Nat. Rev. Mater.* **3**, 18008 (2018).
- Du, N. et al. Design of superior spider silk: from nanostructure to mechanical properties. *Biophys. J.* <https://doi.org/10.1529/biophysj.106.089144> (2006).
- Copeland, C. G., Bell, B. E., Christensen, C. D. & Lewis, R. V. Development of a process for the spinning of synthetic spider silk. *ACS Biomater. Sci. Eng.* <https://doi.org/10.1021/acsbomaterials.5b00092> (2015).
- Simmons, J. R., Xu, L. & Rainey, J. K. Recombinant pyriform silk fiber mechanics are modulated by wet-spinning conditions. *ACS Biomater. Sci. Eng.* <https://doi.org/10.1021/acsbomaterials.9b00504> (2019).
- Madurga, R. et al. Production of high performance bioinspired silk fibers by straining flow spinning. *Biomacromolecules* <https://doi.org/10.1021/acs.biomac.6b01757> (2017).
- Rising, A., Hjalml, G., Engström, W. & Johansson, J. N-terminal nonrepetitive domain common to dragline, flagelliform, and cylindrical spider silk proteins. *Biomacromolecules* **7**, 3120–3124 (2006).
- Hagn, F. et al. A conserved spider silk domain acts as a molecular switch that controls fibre assembly. *Nature* **465**, 239–242 (2010).
- Andersson, M. et al. Biomimetic spinning of artificial spider silk from a chimeric minispidroin. *Nat. Chem. Biol.* <https://doi.org/10.1038/nchembio.2269> (2017).
- Schmuck, B. et al. High-yield production of a super-soluble miniature spidroin for biomimetic high-performance materials. *Mater. Today* **50**, 16–23 (2021).
- Gonska, N. et al. Structure-function relationship of artificial spider silk fibers produced by straining flow spinning. *Biomacromolecules* <https://doi.org/10.1021/acs.biomac.0c00100> (2020).
- Greco, G. et al. Properties of biomimetic artificial spider silk fibers tuned by postspin bath incubation. *Molecules* <https://doi.org/10.3390/molecules25143248> (2020).
- Greco, G. et al. Tyrosine residues mediate supercontraction in biomimetic spider silk. *Commun. Mater.* **2**, 43 (2021).
- Bäcklund, F. G. et al. An image-analysis-based method for the prediction of recombinant protein fiber tensile strength. *Materials* **15**, 708 (2022).
- Weibull, W. A statistical theory of the strength of materials. *Ingenjörsvetenskapsakademiens* **151**, 1–45 (1939).
- Arndt, T., Laity, P. R., Johansson, J., Holland, C. & Rising, A. Native-like flow properties of an artificial spider silk dope. *ACS Biomater. Sci. Eng.* <https://doi.org/10.1021/acsbomaterials.0c01308> (2021).
- Yazawa, K. & Sasaki, U. Forcibly spun dragline silk fibers from web-building spider *Trichonephila clavata* ensure robustness irrespective of spinning speed and humidity. *Int. J. Biol. Macromol.* **168**, 550–557 (2021).
- Otkovs, M. et al. Degree of biomimicry of artificial spider silk spinning assessed by NMR spectroscopy. *Angew. Chemie Int. Ed.* **56**, 12571–12575 (2017).
- Andersson, M. et al. Carbonic anhydrase generates CO₂ and H⁺ that drive spider silk formation via opposite effects on the terminal domains. *PLoS Biol.* **12**, e1001921 (2014).
- Knight, D. P. & Vollrath, F. Changes in element composition along the spinning duct in a *Nephila* spider. *Naturwissenschaften* <https://doi.org/10.1007/s001140100220> (2001).
- Oktaviani, N. A., Matsugami, A., Hayashi, F. & Numata, K. Ion effects on the conformation and dynamics of repetitive domains of a spider silk protein: Implications for solubility and β -sheet formation. *Chem. Commun.* <https://doi.org/10.1039/c9cc03538a> (2019).
- Chen, J., Ohta, Y., Nakamura, H., Masunaga, H. & Numata, K. Aqueous spinning system with a citrate buffer for highly extensible silk fibers. *Polym. J.* **53**, 179–189 (2021).
- Young, R. J., Holland, C., Shao, Z. & Vollrath, F. Spinning conditions affect structure and properties of *Nephila* spider silk. *MRS Bull.* **46**, 1–10 (2021).
- Greco, G., Mirbaha, H., Schmuck, B., Rising, A. & Pugno, N. M. Artificial and natural silk materials have high mechanical property variability regardless of sample size. *Sci. Rep.* **12**, 3507 (2022).
- Arndt, T. et al. Spidroin N-terminal domain forms amyloid-like fibril based hydrogels and provides a protein immobilization platform. *Nat. Commun.* <https://doi.org/10.1038/s41467-022-32093-7> (2022).
- Chan, H. et al. Effect of wet spinning and stretching to enhance mechanical properties of cellulose nanofiber filament. *Int. J. Precis. Eng. Manuf. Technol.* **6**, 567–575 (2019).
- Alagirusamy, R. & Das, A. Conversion of fibre to yarn. in *Textiles and fashion* (ed. Sinclair, R. B. T.-T. F.) 159–189 (Elsevier, 2015). <https://doi.org/10.1016/B978-1-84569-931-4.00008-8>.
- Wagner, J. R., Mount, E. M. & Giles, H. F. Monofilaments. in *Extrusion* (eds. Wagner, J. R., Mount, E. M. & Giles, H. F. B. T.-E. (Second E.)) 585–591 (William Andrew Publishing, 2014). <https://doi.org/10.1016/b978-1-4377-3481-2.00051-x>.
- Weber, W., Yarger, J. L., Albertson, A. E., Teule, F. & Lewis, R. V. Effects of different post-spin stretching conditions on the mechanical properties of synthetic spider silk fibers. *J. Mech. Behav. Biomed. Mater.* **29**, 225–234 (2014).
- Gu, L., Jiang, Y. & Hu, J. Scalable spider-silk-like supertough fibers using a pseudoprotein polymer. *Adv. Mater.* <https://doi.org/10.1002/adma.201904311> (2019).
- Madurga, R. et al. Comparison of the effects of post-spinning drawing and wet stretching on regenerated silk fibers produced through straining flow spinning. *Polymer* **150**, 311–317 (2018).
- Jao, D., Hu, X. & Beachley, V. Bioinspired silk fiber spinning system via automated track-drawing. *ACS Appl. Bio Mater.* <https://doi.org/10.1021/acsbom.1c00630> (2021).
- Gordon, J. E. *The science of structures and materials*, vol. 26. (Choice Reviews Online, 1988).
- Herráez, M., Fernández, A., Lopes, C. S. & González, C. Strength and toughness of structural fibres for composite material reinforcement. *Philos. Trans. R. Soc. A Math. Phys. Eng. Sci.* **374**, 20150274 (2016).

58. Arndt, T. et al. Engineered spider silk proteins for biomimetic spinning of fibers with toughness equal to dragline silks. *Adv. Funct. Mater.* n/a, 2200986 (2022).
59. Zhu, H. et al. Tensile properties of synthetic pyriform spider silk fibers depend on the number of repetitive units as well as the presence of N- and C-terminal domains. *Int. J. Biol. Macromol.* **154**, 765–772 (2020).

Acknowledgements

This work was supported by European Research Council (ERC) under the European Union's Horizon 2020 research and innovation program (grant agreement No 815357), the Center for Innovative Medicine (CIMED) at Karolinska Institutet and Stockholm City Council, Karolinska Institutet SFO Regen (FOR 4-1364/2019), FORMAS (2019-00427), Olle Engkvist stiftelse (207-0375) and the Swedish Research Council (2019-01257) to A.R. G.G. is supported by the Caritro Foundation (prot. U1277.2020/SG.1130) and by Wenner-Gren stiftelse (UPD2021-0047).

Author contributions

B.S., G.G. and A.R. conceived the concept. A.R., J.J., and N.M.P. supervised the project. B.S. produced the protein, performed spinning and tensile testing. G.G. conducted tensile testing and obtained fiber images with SEM. F.G.B. obtained brightfield and polarized light images of the fibers. All authors contributed to the analysis and discussion of the data. B.S., G.G., F.G.B. and A.R. wrote the manuscript, but all authors contributed to the editing process. All authors have given approval to the final version of the manuscript.

Funding

Open access funding provided by Karolinska Institute.

Competing interests

The authors declare no competing interests.

Additional information

Supplementary information The online version contains supplementary material available at <https://doi.org/10.1038/s43246-022-00307-6>.

Correspondence and requests for materials should be addressed to Benjamin Schmuck or Anna Rising.

Peer review information *Communications Materials* thanks Keiji Numata, Jen-Chang Yang and the other, anonymous, reviewer for their contribution to the peer review of this work. Primary Handling Editor: John Plummer. Peer reviewer reports are available.

Reprints and permission information is available at <http://www.nature.com/reprints>

Publisher's note Springer Nature remains neutral with regard to jurisdictional claims in published maps and institutional affiliations.



Open Access This article is licensed under a Creative Commons Attribution 4.0 International License, which permits use, sharing, adaptation, distribution and reproduction in any medium or format, as long as you give appropriate credit to the original author(s) and the source, provide a link to the Creative Commons license, and indicate if changes were made. The images or other third party material in this article are included in the article's Creative Commons license, unless indicated otherwise in a credit line to the material. If material is not included in the article's Creative Commons license and your intended use is not permitted by statutory regulation or exceeds the permitted use, you will need to obtain permission directly from the copyright holder. To view a copy of this license, visit <http://creativecommons.org/licenses/by/4.0/>.

© The Author(s) 2022